Inherently Matched Arrays Over Wide Scan Ranges, Part II: Self-Dual Power Splitters

Roee Geva and Raphael Kastner

Abstract — Self-dual media (SDM) have been shown to enable the design of inherently reflectionless radiating elements for phased array applications with extreme scanning demands. As a natural continuation to this work, we lay here the foundations for an SDM-based feeding network by introducing and simulating SDM-based power splitters as well as a transition from a conventional microstrip to SDM.

1. Introduction

Recently [1], we applied the remarkable property of nonreflection from self-dual media (SDM) [2] to the design of inherently matched phased array elements over large scan ranges. We now proceed to the design of SDM-based power splitters as building blocks for future beamforming networks. These devices are designed in the environment of SDM–transverse electromagnetic (TEM) waveguide. A concept of such a waveguide, used in the sequel, has a square cross section where the upper and lower walls are made of perfect electric conductors and the side walls are perfect magnetic conductors (disregarding for now the effects of possible magnetic metasurfaces described in [1]). As a prerequisite for splitter designs, waveguide bends are suggested and simulated in Section 2. Some configurations of power splitters are then presented in Section 3, and SDM-to-microstrip transitions are shown in Section 4. Conclusions are drawn in Section 5.

2. SDM Bends

A power-dividing network, used for the purpose of feeding an array with SDM-based elements, would preferably be designed in the SDM-TEM waveguiding environment. While bending such waveguides constitute a deviation from the strict SDM condition, it is still advisable to find out any resulting practical limitations with an eye on eventual implementations. To this end, we are examining 90° sharp transitions (see Figure 1a) as well as curved bends whose cascaded combination is seen in Figure 1b. In both configurations, we address bends in both *E*- and *H*-planes.

S-parameters are simulated for two-port networks containing a bend and fed with SDM-TEM ports. Results are shown in Figure 2. For the 90° transition (Figure 2a), the transmission coefficient S_{21} is practically ideal at about 0 dB, while the reflection coefficient S_{11} is under the −20 dB level over the 2 GHz to 20 GHz range. Figure 2b shows the results for the combination of curved bends. Here, the transmission coefficient S_{21} is again near ideal, while the reflection coefficient S_{11} is below −30 dB over the 1 GHz to 10 GHz range. One can arrive at the conclusion that the strict SDM criterion can be somewhat relaxed when it comes to certain designs.

Manuscript received 3 December 2022.

Roee Geva and Raphael Kastner are with the School of Electrical Engineering, Tel Aviv University, 69978 Tel Aviv, Israel; e-mail: kast@tauex.tau.ac.il.

3. SDM Power Splitters

Radiating elements of the type in [1], when incorporated into a phased array system, would be fed by a power-dividing network comprising SDM splitters. One option is direct-aperture-feed (DAF) splitters. These are basically space feeds capable of dividing the energy almost uniformly in a $1{:}N^2$ ratio, $N = 2, 3, \ldots$. It comprises three levels, seen in Figure 3a:

1. The "entrance level" is a section of the SDM-TEM waveguide serves as the conduit that includes the input port plane.
2. The "tapering level" is a flared waveguide of the same type.
3. The split aperture is comprised of an $N \times N$ array of SDM elements, where $N = 2, 3 \ldots$, and terminates the taper; see the front view for the $N = 4$ case in Figure 3b. In the examples below, all central bores share equal dimensions.

The DAF splitter in Figure 3b provides a 1:16 division in a single stage, making it relatively compact and easy to design and model.

The effect of length of the tapering level on power-division performance was investigated in two aspects, namely, *S*-parameter performance and radiation efficiency of the aperture when all elements are open ended and radiating. As a rule of thumb, for linear tapering, reasonable performance will be achieved when the taper length is twice the aperture size. *S*-parameter

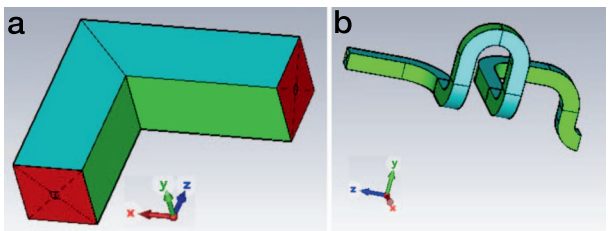

Figure 1. Bends of the SDM-TEM waveguides. (a) 90° transition. (b) Cascaded curved E and H plane bends. Cross sections of waveguides are all 6×6 mm^2.

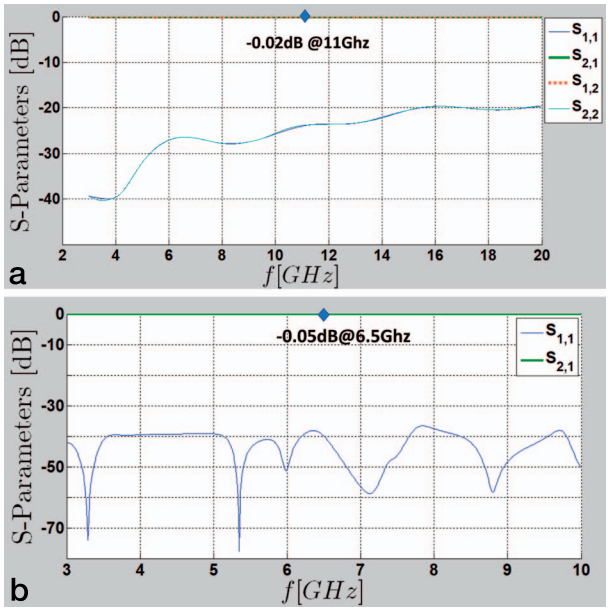

Figure 2. *S*-parameter amplitudes of the bends in Figure 1. (a) 90° bend. (b) Curved E and H plane bends.

performance of both 1:16 ($N = 4$) and 1:64 ($N = 8$) splitters with taper length as per the above-mentioned rule of thumb are shown in Figure 4. As expected, inherently good matching is achieved all over the operational bandwidth. For example, for a 1:64 splitter with the 100-mm taper length (Figures 4c and 4d), the peak-to-peak deviations are 1.6 dB and 48°. In other words, the average difference between adjacent elements is about 0.2 dB and 6°. Performance for two tapering lengths, 15 mm and 50 mm, is shown for the 1:16 splitter in Figure 5. As one may expect, results improve with longer tapers.

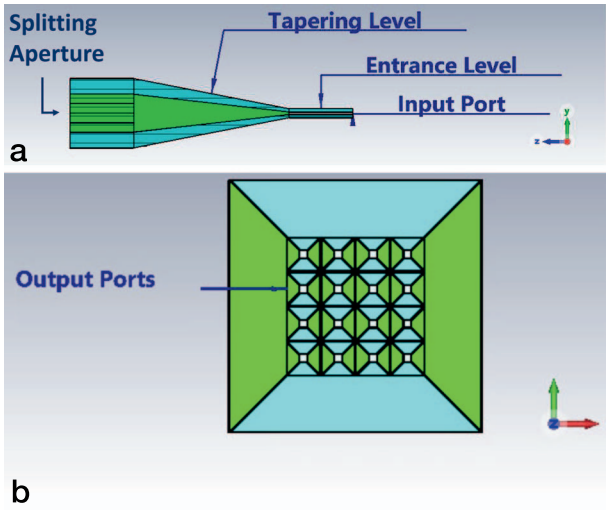

Figure 3. Direct-aperture-feed (DAF) splitter. (a) Side view: DAF levels. (b) Front view: splitting aperture. Each output port is 6 mm^2 × 6 mm^2 wide.

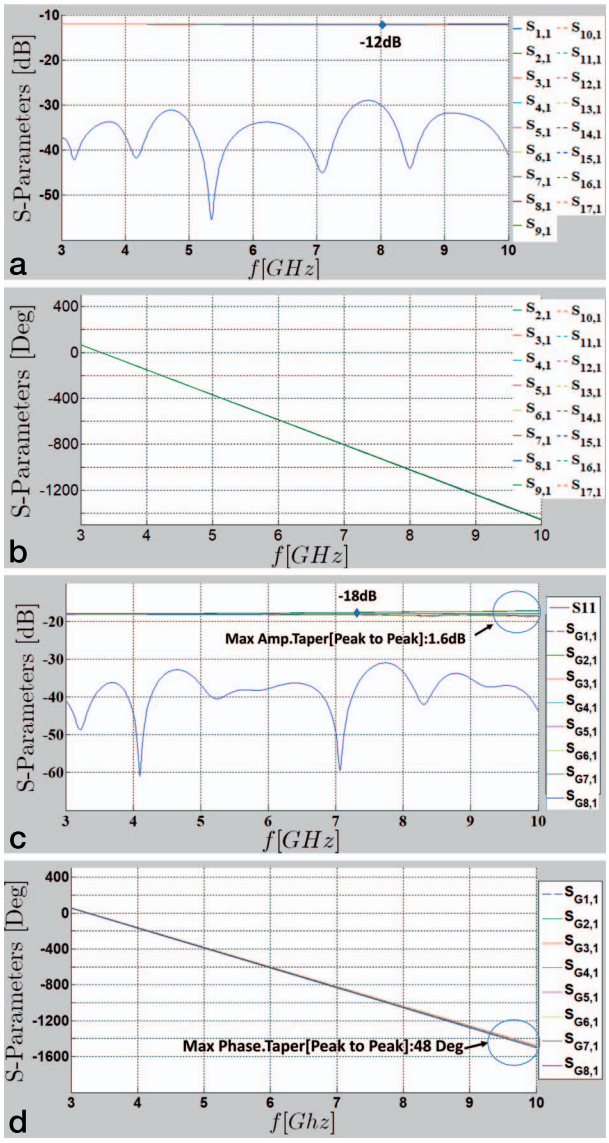

Figure 4. *S*-parameter performance for 1:16 and 1:64 DAF splitters. In (a) and (b), all ports are shown. In (c) and (d), ports have been grouped; each group shares the same distance from the center of the aperture and the same amplitude and phase. The worst case for the 1:64 splitter occurs at the highest frequency, marked with circles in (c) and (d).

When a higher split ratio is desired, a single stage may be too bulky for this rule-of-thumb implementation. Partitioning into two stages or more may be then preferred. In Figure 6, a 1:256 ratio is achieved in two stages. The initial stage with a 1:4 ratio is connected to the second stage of four 1:64 splitters via a network of waveguides and bends of the type in Section 2.

4. Microstrip to SDM-TEM Waveguide Transition

To connect with conventional RF devices, a transition is proposed as follows. We note that the bore

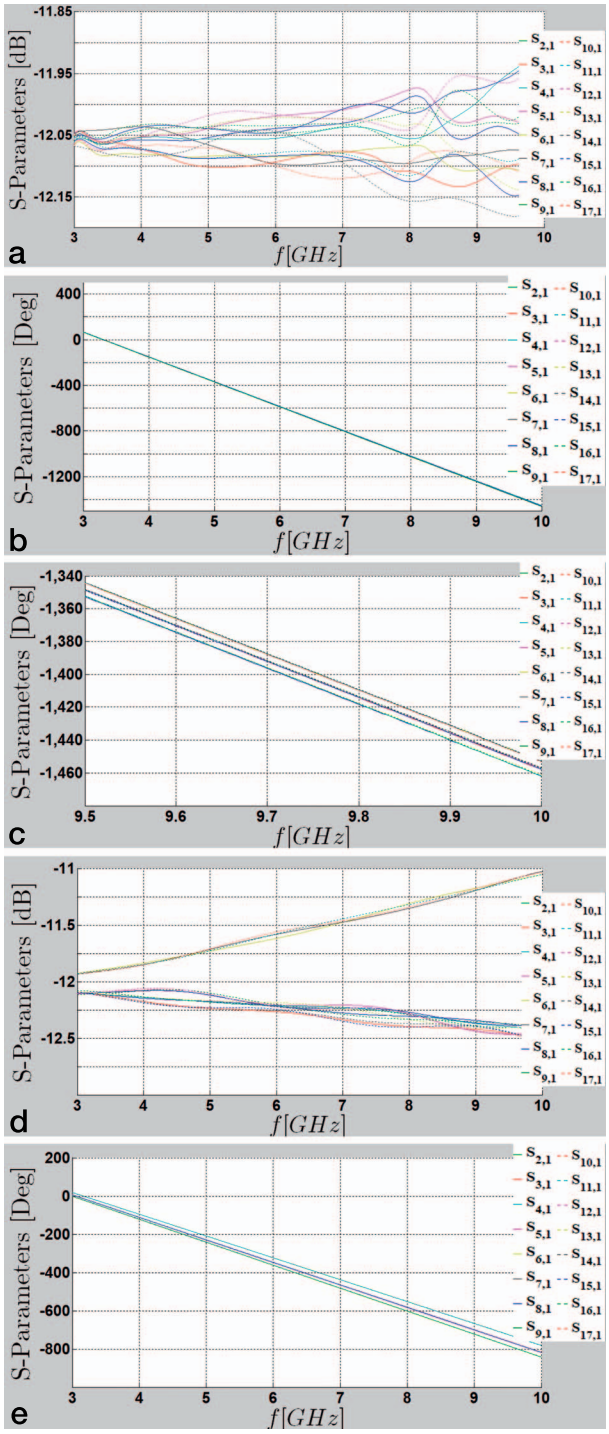

Figure 5. *S*-parameter performance for two lengths of taper in the 1:16 splitter. (a) *S*-parameters amplitude (dB) for a 50 mm taper. (b) *S*-parameter phase (°) for a 50 mm taper. (c) An enlargement of Figure 5(b) for the 9.5 GHz to 10 GHz range. (d) *S*-parameters amplitude (dB) for a 15 mm taper. (e) *S*-parameter phase (°) for a 15 mm taper.

within the radiating element of [1] supports a TEM mode with a characteristic impedance of $Z_c = 377\ \Omega$. Since microstrip lines with the same impedance are impractical, we are proposing a TEM horn [3] as a

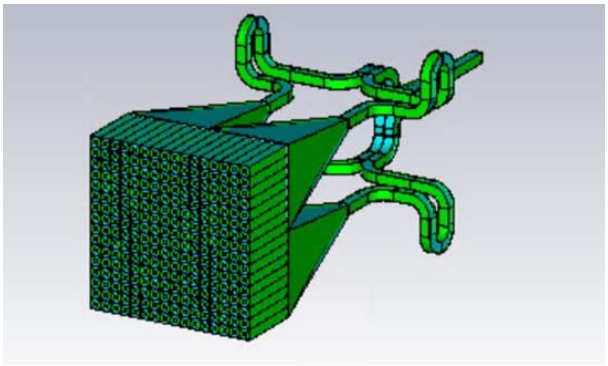

Figure 6. A splitter model involving bends and tapers to reduce the overall taper lengths. Superfluous bends are included for the sake of validating bend robustness.

tapered transition between the two lines; see Figure 7. The aperture of the TEM horn that interfaces directly with the SDM should support the fundamental TEM mode only. The cutoff wavelength of the next-higher-order mode is given by $\lambda_c = 2d$, where d is the TEM horn height. In our operational bandwidth of 3 GHZ to 10 GHz, the dimensions of this output port are limited to 15 mm. As the impedance at any point along the horn is given by $Z_{\text{horn}}(z) = 120\pi \frac{d(z)}{W(z)}$, the requirement for 377-Ω line impedance at its output port implies that $d_{\text{out}} = W_{\text{out}}$. The width and height at any other point along the TEM horn are governed by an exponential taper. The TEM horn may be fed in the standard way by using, for example balun-microstrip line. With the height and width at the output already set, the sole unknown left to determine is the input impedance, which should fit the feeding waveguide. In this proposed feeding method, the entrance level for each SDM element is constructed of a standard waveguide (such as balun microstrip). Other feeding methods, such as gap waveguides, are under consideration.

The SDM itself, now uniformly illuminated by a normal incident plane wave, is transparent to this feeding structure. Representative *S*-parameter results for the TEM horn alone are shown in Figure 8a for an input

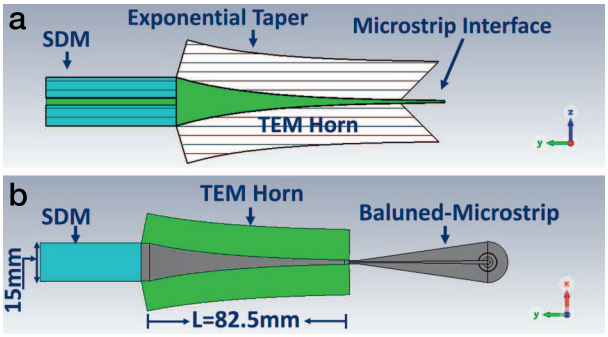

Figure 7. Microstrip-to-SDM transition. (a) SDM fed with TEM-horn side profile. (b) SDM feed via a microstrip line.

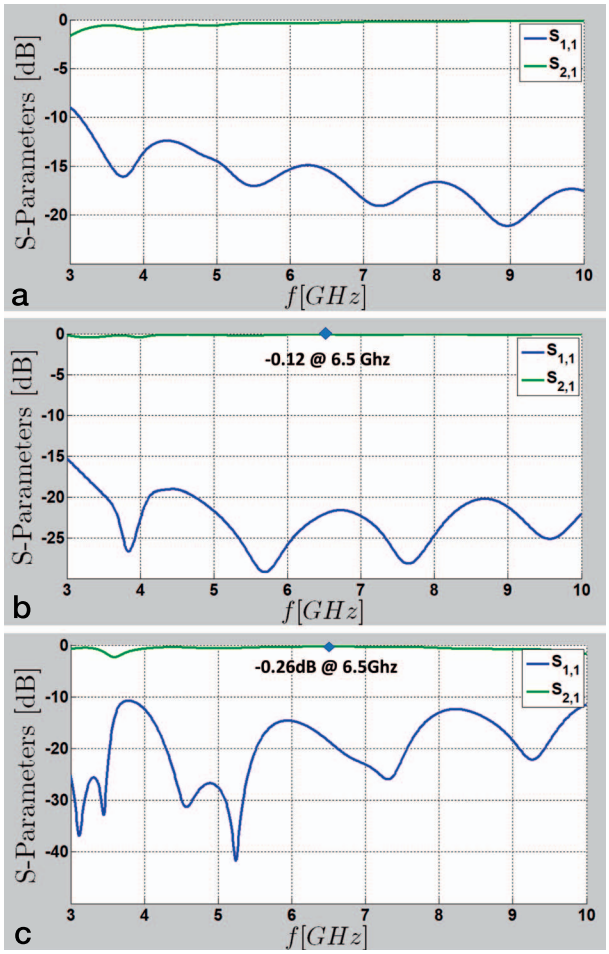

Figure 8. *S*-parameters of the microstrip-to-SDM transition seen in Figure 7. (a) *S*-parameters of the TEM horn itself as input impedance is transformed from 130 Ω to 377 Ω at the SDM interface. (b) *S*-parameters of the TEM-horn to SDM transition. (c) Example of feeding via microstrip line. *S*-parameters for microstrip to TEM-horn to SDM.

impedance of 130 Ω, while the TEM-horn-SDM level performance is shown in Figure 8b. An example of feeding the TEM-horn-SDM combination via a microstrip line is shown in Figure 8c. In this case, the performance is determined mostly by the microstrip-to-TEM-horn interface.

5. Conclusions

Practical bandwidths of the devices proposed above would eventually depend on the actual realization of magnetic walls as metasurfaces. In [1], we picked certain options from the abundant literature on this subject. It is anticipated that additional passive devices, such as hybrid couplers, can be devised and incorporated into SDM-based Butler matrices. Planar Rotman-type lenses are also deemed feasible. The issue of active components, such as phase shifters and switches, remains outside the scope of this work for now. At present, one can suggest a connection between conventional devices and the SDM by the microstrip-to-SDM transition described in Section 4. Also, nonuniform amplitude distributions across the aperture, needed for pattern synthesis, are left for future work.

6. References

1. R. Geva and R. Kastner, "Inherently Matched Arrays Over Wide Scan Range, Part I: Self-Dual Radiating Element," companion paper in this volume.
2. N. Mohammadi Estakhri, N. Engheta, and R. Kastner, "Electromagnetic Funnel: Reflectionless Transmission and Guiding of Wave Through Subwavelength Apertures," *Physical Review Letters*, **124**, 22, January 2020, p. 033901.
3. K. Chung, S. Pyun, and J. Choi "Design of an Ultrawide-Band TEM Horn Antenna With a Microstrip-Type Balun," *IEEE Transactions on Antennas and Propagation*, **53**, 10, October 2005, pp. 3410-3413.